ACS OMEGA

http://pubs.acs.org/journal/acsodf

Article

Biomimetic Inorganic Nanoparticle-Loaded Silk Fibroin-Based Coating with Enhanced Antibacterial and Osteogenic Abilities

Yunpeng Zhang,*,‖ Xiaorong Chen,‖ Yuan Li, Tian Bai, Chen Li, Lingyan Jiang, Yu Liu, Changying Sun, and Wenhao Zhou*

Cite This: *ACS Omega* 2021, 6, 30027−30039

Read Online

ACCESS | Metrics & More | Article Recommendations

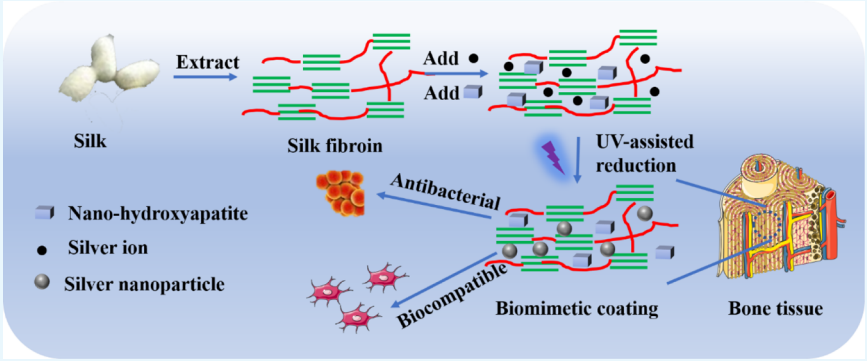

ABSTRACT: Poor osseointegration and infection are the main reasons leading to the failure of hard tissue implants; especially, in recent years, the failure rate has been increasing every year owing to the continuously increasing conditions such as injury, trauma, diseases, or infections. Therefore, the development of a biomimetic surface coating of bone tissues with antibacterial function is an effective means to improve bone healing and inhibit bacterial infection. Mimicking the natural bone, in this study, we have designed a silk fibroin (collagen-like structure)-based coating inlaid with nanohydroxyapatite (nHA) and silver nanoparticles (AgNPs) for promoting antibacterial ability and osteogenesis, especially focusing on the bone mimetic structure for enhancing bone health. Observing the morphology and size of the composite nanoparticles by transmission electron microscope (TEM), nHA provided nucleation sites for the formation of AgNPs, forming an nHA/AgNP complex with a size of about 100−200 nm. Characterization of the nHA/Ag-loaded silk fibroin biomimetic coating showed an increased surface roughness with good density and compact performances. The silk fibroin-based coating loaded with uniformly distributed AgNPs and nHA could effectively inhibit the adhesion of *Staphylococcus aureus* on the surface and, at the same time, quickly kill planktonic bacteria, indicating their good antibacterial ability. *In vitro* cell experiments revealed that the biomimetic silk fibroin-based coating was beneficial to the adhesion, spreading, and proliferation of osteoblasts (MC3T3-E1). In addition, by characterizing LDH and ROS, it was found that the nHA/Ag complex could significantly reduce the cytotoxicity of AgNPs, and the osteoblasts on the coating surface maintained the structure intact.

1. INTRODUCTION

Records show that the postoperative implantation failure rate of titanium-based implant materials (biologically inert) is about 10%, and the two main reasons for implantation failure are poor osseointegration and infection.[1,2] The reasons for the poor osseointegration of titanium-based implants after surgery include their higher elastic modulus than that of the natural bone tissue, and the "stress shielding" effect produced will lead to biomechanical mismatch during implantation.[3] Second, the titanium-based implant lacks the necessary biological activity and osteoinductive activity, and it is not easy to form a biological bond with natural bone tissue.[4] There is also a close connection between the infection and osseointegration. Studies have pointed out that the occurrence of early infection will also lead to a significant increase in the rate of osseointegration.[5,6] If the implant has a certain antibacterial ability, this is conducive to cell adhesion, proliferation, and differentiation, improving osseointegration. In summary, although the medical titanium−tantalum alloy has excellent integrated mechanical properties and wear resistance and corrosion resistance, the

Received: August 30, 2021
Accepted: October 15, 2021
Published: October 28, 2021

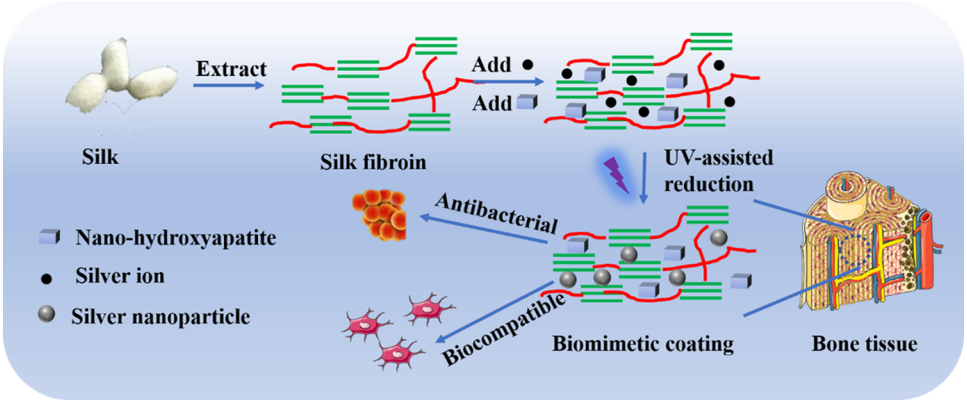

Figure 1. Illustration of the preparation process of biocompatible and antibacterial coatings.

lack of vital bone-promoting activity and antibacterial ability limits its application in the field of hard tissue implantation.[7] The osseointegration of the implant and the occurrence of infection play a crucial role. Therefore, adjusting the surface properties of titanium−tantalum alloy implants through effective surface modification methods to achieve good osseointegration and antibacterial adhesion has become a hot issue that needs to be studied and resolved.

The clinical performance can be largely enhanced by the bioactive coating on the metallic orthopedic implants including decelerating the surgical infection and increasing the rate of osseointegration.[8] The optimization of a bioactive implant coating needs a series of improvements including the material composition, the coating structure, the topography of the surface, and the manufacturing methods. Nanohydroxyapatite (nHA) has been verified as a greatly promising bioactive coating material owing to its ability to stimulate osteogenesis and osseointegration.[9] However, an inflexible coating is produced by the application of individual nHA due to its intrinsic brittleness.[10] This problem can be solved by the integration of macromolecules and nHA, yielding a soft and flexible composite structure. Moreover, biomedical coatings widely make use of the natural macromolecules with nHA for their particular nature including excellent film-forming property and enhanced interaction among cells.[11]

Biomimetic nanocomposites that are highly structurally similar to the natural bone minerals are studied to be produced by biomimetic approaches with template molecules like silk fibroin (SF) and collagen.[12,13] Also, these nanocomposites produced by regulating the usage of protein templates are able to lead to new mineral deposition, promoting the cell proliferation and adhesion, resulting in speedy osseointegration and bone regeneration, thanks to their high biological activity, which have extensive application in bone implantation materials.[14,15] Significantly different from other natural macromolecular polymers is that SF is a better choice of biomaterials for bone regeneration.[16,17] The structure of SF's fibrin is very similar to Col I, an important organic component in the bone microstructure. In addition, the amorphous connections in the SF's β-sheet structure have anionic properties similar to those of noncollagen proteins and can be used as nucleation sites for nHA.[18] In addition, the SF's β-sheet secondary structure endows it with excellent mechanical properties, minimal cytotoxicity, and immunogenicity. In addition, even in a nonosteogenic medium, the SF-based coating can promote the spreading of osteoblast filopodia and the stable adhesion of lamellar pseudopods, along with the continuous accumulation of mineralized nodules on the surface.[19] Thanks to the good bone-promoting properties and biological safety of SF, SF-based coatings are widely used for surface modification of hard tissue implant materials.

Antibacterial coatings loaded with silver are broadly applied to resist biomedical device-associated infections (BAIs) due to their good properties such as good inhibition to the biofilm, well-behaved stability, and a broad antimicrobial spectrum.[20] AgNPs are proved to have better antibacterial performance attributed to the combined effects of nanoparticles' physical properties and eluted silver ions. AgNPs are assumed to be able to cling to the surface of bacteria, adjusting their membrane nature and imposing damage on DNA across the membrane.[21] Also, the silver ions released by AgNPs can combine with thiol-containing proteins to reduce their physiological activity, thereby exhibiting excellent antibacterial properties.[22] Bacteria have poor resistance to silver because AgNPs work with several bactericidal mechanisms at the same time. It has been proved by research studies that the low-concentration and sustaining silver ion release is conducive to facilitating osteoblasts' differentiation and bone healing.[23−25]

Based on the concept of a bone-microstructure-biomimetic coating, an nHA/AgNP-loaded SF-based coating wasbuilt for rapid bone induction regeneration and resistance to bacterial infections (Figure 1). To improve the bonding force between the SF-based coating and the substrate, inspired by marine mussels, an assistant polydopamine (PD) layer has been introduced, which has been widely used as an important and universal building block for modifying the interface of biological materials. With the aid of PD, a rigid nHA/AgNP-loaded SF coating could be easily fabricated on Ti. The goals of the current work are as follows: (1) The treatment and characterization of nHA and AgNPs coated by SF, their structural integrity, and dispersion uniformity; (2) the development and characterization of nHA/Ag-loaded silk fibroin coatings, their surface roughness, chemical properties, and wettability that has a significant impact on their biological activity; (3) according to their antiadhesion and plankton-killing properties, the evaluation of the antibacterial ability of the coating containing AgNPs; and (4) research studies on the adhesion, proliferation, LDH, and ROS to reflect how MC3T3 cells respond to the nHA/AgNP-loaded SF-based coating. Although titanium-based hard tissue implants with biologically inert surfaces were widely used, bacterial infection and poor osseointegration were still the main reasons for their

https://doi.org/10.1021/acsomega.1c04734
ACS Omega 2021, 6, 30027−30039

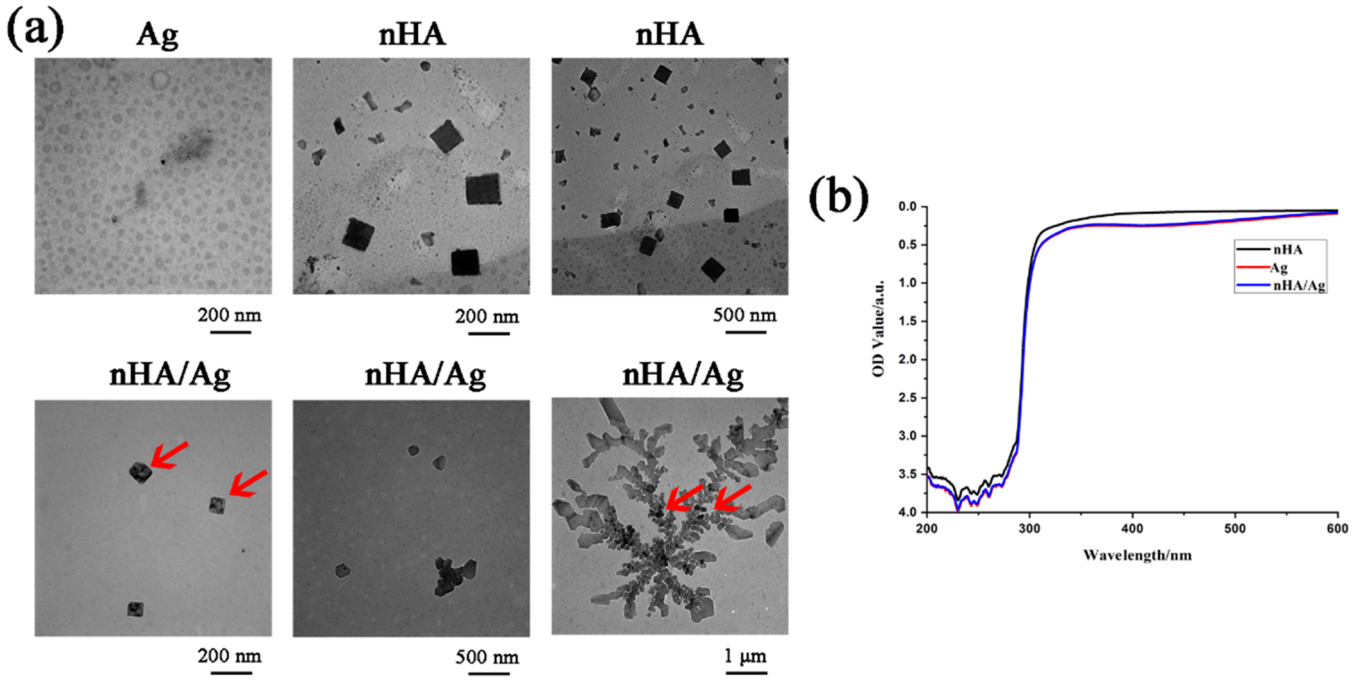

Figure 2. (a) TEM images of Ag, nHA, and nHA/Ag composites with 1 h UV irradiation time; the red arrow indicates the nHA/AgNP complex. (b) UV−vis spectra of nHA, Ag, and nHA/Ag.

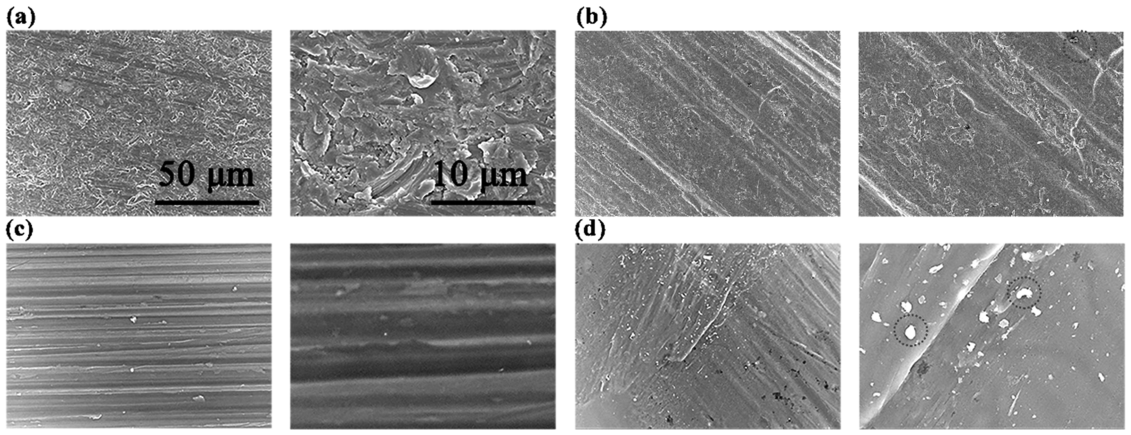

Figure 3. Morphology and the structure of the coating: SEM images of TC4 (a), nHA (b), Ag (c), and nHA/Ag (d).

implantation failure. Therefore, in this study, nHA/AgNP-loaded SF-based coatings were used for surface modification of titanium-based implants. It is expected to achieve anti-infective effects at the initial stage of implantation (<7 days) and good new bone formation and bone fusion within 1 month of implantation. (Figure 1

2. RESULTS

2.1. Detection of the nHA/AgNP Morphology. The morphology and particle size of the inorganic particles nHA and AgNPs were observed through transmission electron microscopy (TEM) images (Figure 2a). Obviously, AgNPs were spherical with a particle size of about 40 nm, while nHA showed a cubic structure with a size of about 100 nm. Interestingly, as indicated by the red arrow, some AgNPs utilized nHA as a nucleation site to form a new type of nHA/AgNP complex with a size of about 100 nm. It was inevitable to observe the phenomenon of nanoparticle aggregation, but this new complex also exhibited new and unique properties compared with nHA and AgNPs. Furthermore, the dendritic structure appeared in the TEM image enlarged by 1 μm, which indicated that the conformation of SF had changed. As verified,[26] when the composition and concentration of the solution changed, the SF conformation would also change due to the change in chargeability. In the changing process, nanoscale microspheres were first formed, and the microspheres were further fused to form a fibrous structure, and finally developed into a dendritic structure, as observed by TEM. Fourier transform infrared (FTIR) deconvolution could be applied to analyze the conversion of the secondary structure of SF, which was involved in the formation of a dendritic structure. In short, the dendritic structure was conducive to the uniform dispersion of nHA and AgNPs to perform their functions. As shown in Figure 2b, the 450 nm SPR band in the UV−vis spectrum represents the presence of AgNPs, confirming the successful recombination of nHA and Ag.

The reducing ability of tyrosine in an amino acid sequence of SF allowed AgNPs to be obtained *in situ*. At the same time,

https://doi.org/10.1021/acsomega.1c04734
ACS Omega 2021, 6, 30027−30039

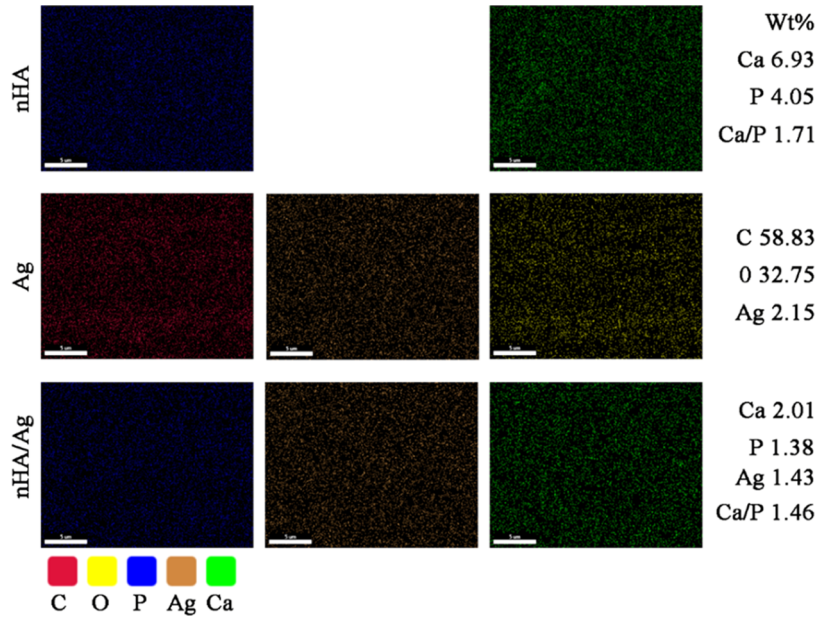

Figure 4. EDS analysis of different coatings.

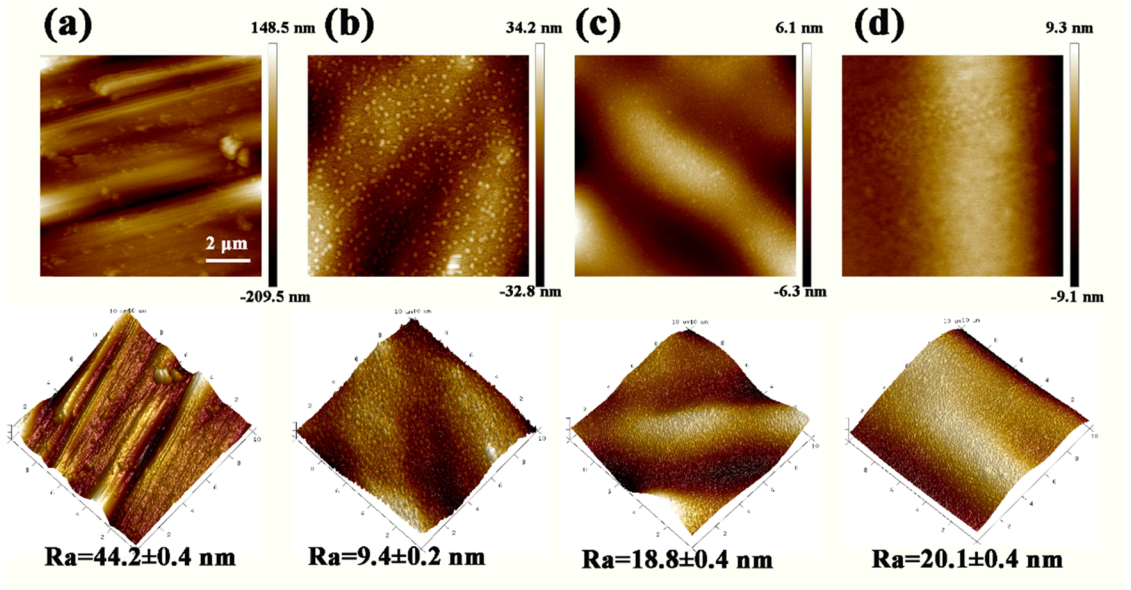

Figure 5. AFM topographical images and roughness values of (a) TC4, (b) nHA, (c) Ag, and (d) nHA/Ag.

SF owned the properties of a stabilizer to guarantee the uniform distribution of AgNPs and nHA. (Figure 2a).[27] Research has confirmed that SF shows the ability to reduce metal ions *in situ*, including nanogold and nanosilver, which is environmentally friendly and morphologically controlled.[28] Following this approach, the mixed solution (SF/nHA/Ag ions) was placed under UV to form an SF-based biomimetic coating; finally, well-distributed nHA/AgNP-loaded coatings were prepared. The obvious change from colorless to yellow in the mixed solution was an optical indicator of the formation of AgNPs. Then, through the UV spectrum (Figure 2b), it was observed that the absorption band near 450 nm corresponded to the formation of AgNPs, which was consistent with the TEM results. Also, the characteristic peaks did not shift, indicating that the nanoparticles did not agglomerate, reflecting the stabilizing ability of SF. SF has been proved to be a stabilizer to maintain the biological activity of active molecules for a long time.[29] The SF-based biomimetic coating formed in this way was beneficial for the long-term bioactivity of nHA and AgNPs.

2.2. Observation of the Morphology of the Biomimetic Coating. Scanning electron microscopy (SEM) observation was utilized to check the surface morphology and the microstructure of the SF-based coatings. As shown in Figure 3a, the surface morphology of polished TC4 was rough, which displayed different degrees of oxide film wrinkles. In contrast, the surface of the nHA and Ag coatings (Figure 3b,c) was relatively flat, and there were obvious cubic-shaped nHA and AgNPs on the surface. After the nHA/Ag coating (Figure 3d) was constructed on the surface, the scratches were not visible, and a large number of nHA/Ag complexes of less than 1 μm were distributed on the surface.

https://doi.org/10.1021/acsomega.1c04734
ACS Omega 2021, 6, 30027−30039

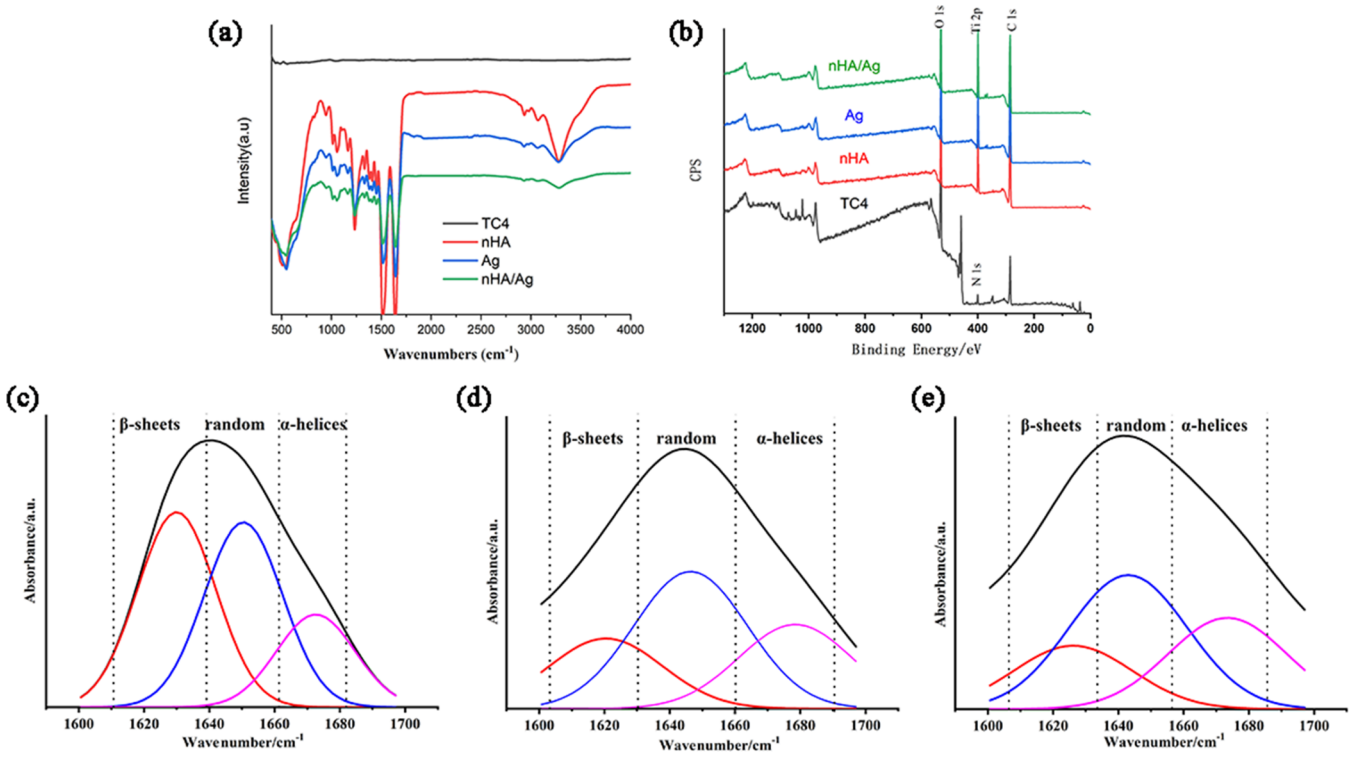

Figure 6. Chemical composition of SF-basedcoatings. (a) Infrared spectra and (b) XPS survey spectra. XPS spectra of amide I deduced after Fourier self-deconvolution of nHA (c), Ag (d), and nHA/Ag (e).

Figure 4 shows the energy dispersive spectroscopy (EDS) maps of surface elemental distribution. Compared with the nHA and Ag groups, the elements of the nHA/Ag group underwent significant changes. Ca/P reduced from 1.71 to 1.46, and the proportion of silver reduced from 2.15 to 1.43%, which meant that the addition of nHA showed a significant impact on the process of reducing silver ions by SF. Research[28] has shown that the mixing of inorganic substances would affect the reduction properties of SF, which was due to the changes in the electrification and conformation of SF. As observed by TEM, some AgNPs used nHA as a nucleation site to form a new nHA/AgNP complex, which was not only helpful for reducing the biological toxicity of AgNPs but also beneficial for exerting the biological properties of the complex.

As shown in Figure 5, the surface morphology and roughness measurement values (Ra) of TC4, nHA, Ag, and nHA/Ag samples were characterized by atomic force microscopy (AFM). Obviously, the surface of TC4 was rough, and many parallel scratches caused by polishing could be clearly observed. In comparison, the surface roughness of the nHA coating (Figure 5b) was the lowest and relatively flat. The surface of the Ag coating (Figure 5c) was also faintly visible with polishing scratch traces. The surface of the nHA/Ag coating shown in Figure 5d is flat, but the roughness is increased due to the formation of nHA/AgNP complexes. Their roughness was 44.2 ± 0.4, 9.4 ± 0.2, 18.8 ± 0.4, and 20.1 ± 0.4 nm, respectively. Surface roughness, as one of the important surface properties of implant materials, presented an important impact on the hydrophobicity and protein adsorption characteristics of the surface. At the same time, studies[30] have pointed out that the surface roughness would affect the spreading and differentiation of osteoblasts on the surface. The surface was too flat and rough, which was not conducive to its contact with cells. In contrast, the surface with a roughness of 20−30 nm was most suitable for osteoblasts. Therefore, the nHA/Ag group showed the best roughness morphology.

2.3. Chemical Property Testing of nHA/AgNPs and Coating. FTIR and X-ray photoelectron spectroscopy (XPS) were utilized to analyze the chemical compositions and characteristic groups of the SF-based coatings. According to the FTIR results (Figure 6a), in addition to the characteristic absorption of −OH at 3450 cm^{-1} for nHA, the positions of the obvious characteristic peaks of nHA, Ag, and nHA/Ag coatings basically overlapped, indicating that increasing Ag and nHA components did not have a significant impact on the SF-based coatings. Studies[31] have shown that the content of the secondary structure of silk fibroin has a significant impact on its physical and chemical properties. It was generally believed that the higher the content of the α-helix structure, the less brittleness of the SF-based coating and the better the wettability. The adjustment of certain external conditions (pH, temperature, and inorganic matter) to realize the mutual transformation between β-sheet and α-helix structures conveniently adjusted the performance of SF-based coatings. In this study, the deconvolution method was used to deconvolve the characteristic peaks of SF 3600−3700 cm^{-1} to obtain the secondary structure ratio (Figure 6c−e). Obviously, compared to the nHA (18%) and Ag (21%) coatings, the α-helix structure content of the nHA/Ag coating was significantly increased to 26%, which meant that the coating displayed lower brittleness and better toughness and wettability, whereas, this feature was conducive to the bonding between the coating and the substrate. As shown in Figure 6b, XPS spectroscopy was used to identify the chemical elements and chemical state information of the SF-based coatings. The distinct characteristic peaks at 531.0, 289.3, and 399.0 eV correspond to O 1s, Ti 2p, and C 1s, respectively. The

https://doi.org/10.1021/acsomega.1c04734
ACS Omega 2021, 6, 30027−30039

successful construction of SF-based coatings resulted in the characteristic peaks of the Ti substrate being significantly weaker or even disappearing.

2.4. Wettability of the SF-Based Coating. As shown in Figure 7, the contact angle (CA) method was applied to check

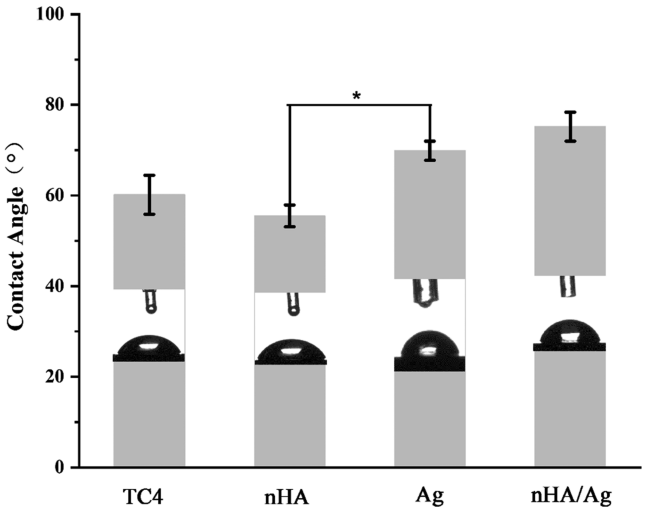

Figure 7. Contact angle of different samples.

the hydrophilicity of the functional coatings. The higher the CA value, the more hydrophobic the surface of the material. According to the CA results, the contact angle of the nHA layer reduced from 76.2 to 58.6° compared with the Ag layer, indicating that nHA was conducive to the improvement of hydrophilicity. In contrast, the CA value of nHA/Ag was slightly higher than that of TC4 because the formation of nHA/AgNP complexes increased the roughness, as shown by AFM.

2.5. *In Vitro* Antibacterial Evaluation. After incubating the SF-based coatings with *S. aureus* in an LB medium for 1 day, the final OD value is shown in Figure 8a,b. Due to the rapid propagation of *S. aureus*, the OD values in the TC4 and nHA groups both exceeded 0.4. On the contrary, the bactericidal ability of the Ag group was slightly improved, and thanks to the formation of nHA/AgNP complexes with a potential synergetic effect, the OD of the nHA/Ag group was close to 0. No matter on the surface or in the suspension, the bactericidal ability of the nHA/Ag coating was close to 100%. Similarly, in Figure 8c, when the coating was loaded with nHA, the colonies of *S. aureus* on the agar plate were slightly reduced, indicating that nHA presented an antibacterial effect but not obvious. In contrast, the number of colonies on the Ag coating was greatly reduced to less than 20, proving that AgNPs owned excellent antibacterial properties. Further, the antibacterial efficiency of nHA/Ag was greatly improved, and no *S. aureus* adhered to the surface. In addition, the morphology of the bacteria and the integrity of the cell membrane were observed by SEM (Figure 8d). Bacteria were easy to attach, proliferate, and aggregate on TC4 and nHA, and presented a full spherical shape with a complete membrane structure. However, the cell membrane of *S. aureus* attached to the Ag coating, especially the nHA/Ag coating, displayed obvious defects, showing wrinkles and depressions. It was clearly visible that both the nHA coating and the Ag coating showed different degrees of defects after cocultivation with the bacterial solution for 1 day. These small holes would adversely affect the stability of the entire film. When the nHA/Ag coating was uniform and compact, there was no obvious damage, which meant that the coating was more stable and long-lasting in comparison, and it was better to bond with the TC4 substrate. Furthermore, the confocal observation obtained the dead/alive fluorescent image of the bacteria to visually present the survival status of the bacteria. As shown in Figure 8e, most bacteria on the surface of TC4 and nHA were active (green) and tend to aggregate. In contrast, the number of individual bacteria on the surface of Ag was significantly reduced, but most of the bacteria that adhered were dead (red). Only on the surface of the nHA/Ag coating, no live bacteria were observed but only a few dead bacteria.

The development of drug-loaded antibacterial coatings on the surface of hard tissue implants is mainly aimed at the elimination of the most relevant bacterial strains related to implant-related infections, including MRSA.[32−34] The related bacteria causing infections are increasingly becoming a clinical thorny problem, including *S. aureus* and *Pseudomonas aeruginosa*, which easily form a complete biofilm on the surface of the implant.[35] Researchers have extensively discussed the antibacterial mechanism of AgNPs, and it is agreed that the antibacterial efficacy of AgNPs is significantly higher than that of Ag^+, which benefits from the complex sterilization mechanism of AgNPs, including contact killing and ion-mediated sterilization.[36,37] As verified, AgNPs can slowly release Ag^+, forming a local high-concentration Ag^+ environment, which is also the main source of AgNP cytotoxicity.[38,39] However, studies have shown that the antibacterial activity of AgNPs not only comes from the Ag^+ released but the natural properties of the nanoparticles also make an outstanding contribution..[40] It can be clearly seen through SEM and TEM that AgNPs can attach to the cell membrane of bacteria, destroy membrane proteins, change the permeability of the membrane, and at the same time, damage its biological functions by interacting with phosphorus and sulfur-containing compounds (such as DNA). AgNPs can attack the respiratory chain of bacteria, affect the process of mitosis, and ultimately lead to the death of bacteria. It is worth mentioning that AgNPs can also effectively kill planktonic bacteria, with antibacterial mechanisms similar to sessile bacteria, which is essential for clinical infection prevention.[41] The antibacterial test results showed that the bone bionic SF-based coating loaded with nHA/Ag could quickly kill *S. aureus* adhered to the surface, and at the same time, it owned a high-efficiency killing effect on the planktonic bacteria. As shown in Figure 8d, the complete bacterial membrane structure should be spherical, and due to the presence of membrane proteins, it should display a more obvious charging phenomenon. For example, the bacteria on the surface of TC4 were white and spherical, while with a sharp contrast on the surface of the nHA/Ag coating, the bacteria appeared flat and dull, which meant that the membrane structure of the bacteria was severely damaged and the bacteria were died. Therefore, AgNPs could destroy the membrane structure of bacteria, causing leakage of the contents, which, in turn, led to the death of bacteria. The live/dead staining results (Figure 8e) displayed that all bacteria adhered on the surface were dead bacteria, and the number was quite small, indicating that the coating surface had a certain self-cleaning ability. Interestingly, the addition of nHA significantly improved the antibacterial efficiency of AgNPs, which could be attributed to the following two points: First, nHA could provide sites for the growth of nanosilver. TEM

https://doi.org/10.1021/acsomega.1c04734
ACS Omega 2021, 6, 30027−30039

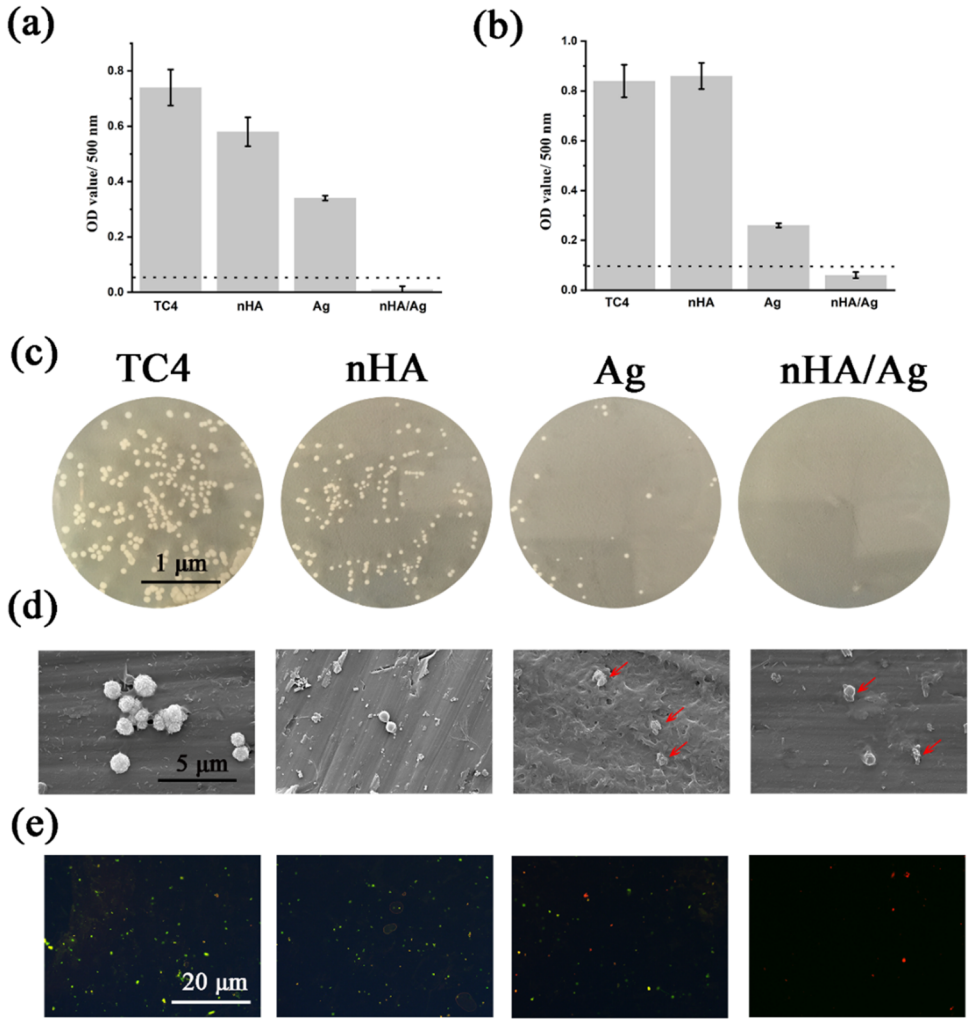

Figure 8. Antibacterial activity of different samples against *S. aureus* after 24 h of incubation (1×10^8 CFU/mL). (a) Coating surface, (b) in liquid, (c) quantitative measurement by the coating method, (d) typical bacterial morphology; the red arrow marks the broken bacterial membrane, and (e) live (green)/dead (red) status.

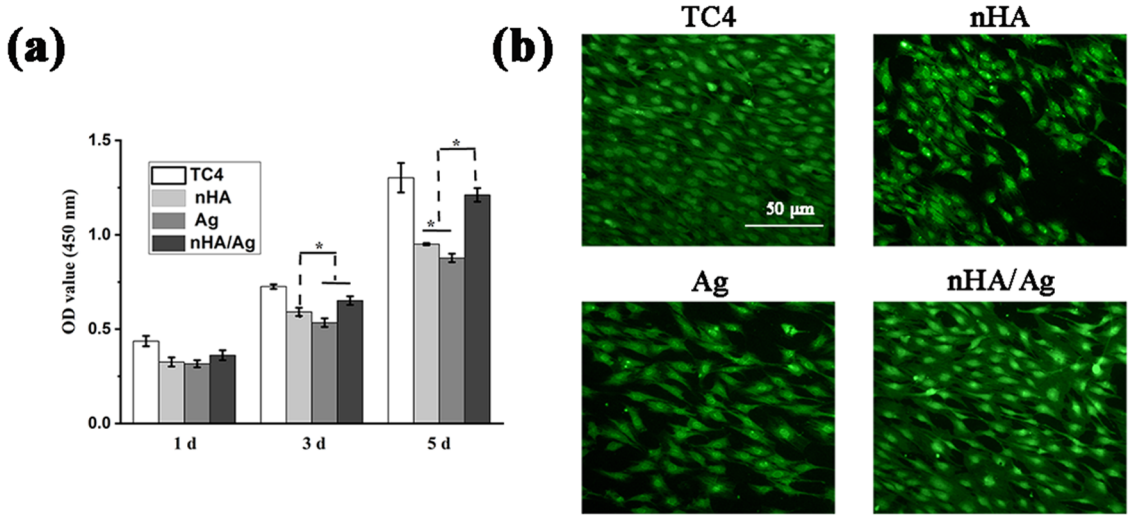

Figure 9. (a) Cell proliferative activity and (b) fluorescence microscopy observation of cytoskeletal actin fibers (green) on different coatings for 5 days.

(Figure 2a) showed that the resulting nanosilver had a smaller particle size. The smaller the particle size, the higher the antibacterial efficiency of AgNPs. Another reason was that the presence of nHA/AgNP complexes led to a locally high-concentration area of Ag^+. nHA provided a site for local aggregation of AgNPs, greatly improving the antibacterial

https://doi.org/10.1021/acsomega.1c04734
ACS Omega 2021, 6, 30027−30039

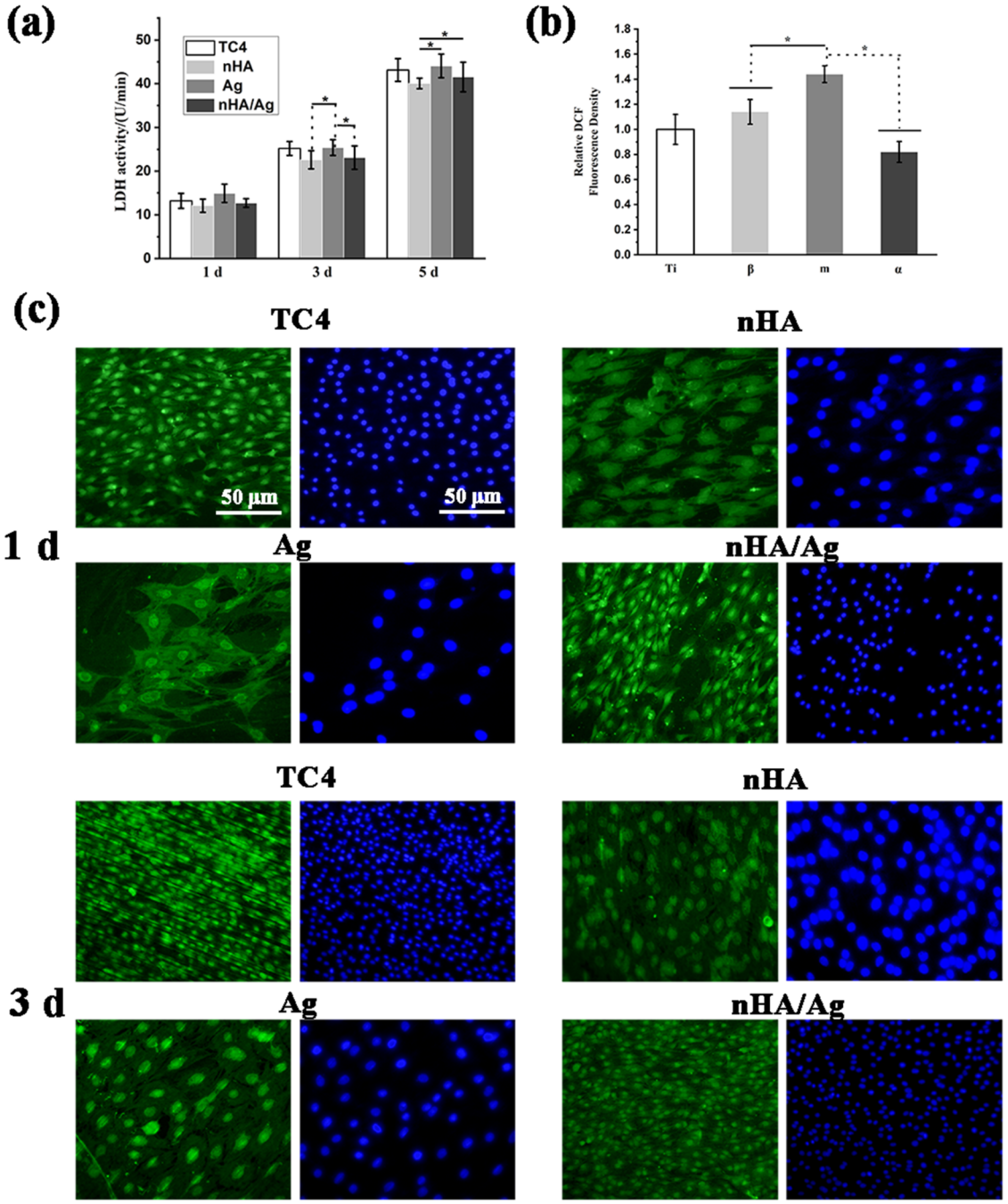

Figure 10. (a) LDH activity for 1, 3, and 5 days; (b) ROS quantitative results of LDH fluorescence density; and (c) fluorescence microscopy observation of cytoskeletal actin fibers (green) and nuclei (blue) on TC4, nHA, and nHA/Ag surfaces for 1 and 3 days.

efficacy of AgNPs. Therefore, the bionic coating exhibited excellent antibacterial ability and could effectively prevent the occurrence of implantation infection.

2.6. Evaluation of Biocompatibility of the SF-Based coating. CCK-8 assay (measuring mitochondrial activity) was performed on days 1, 3, and 5 to evaluate the proliferation of MC3T3-E1 cells on different SF-based coatings. As shown in Figure 9a, on the first day, the cell proliferation on the surface of the nHA/Ag structure coating was slightly lower than that of the TC4 group, but the cell proliferation presented a good time dependence, which meant that there were no obvious cells in the nHA/Ag structure coating toxicity. After 5 days of cocultivation, the number of cells on the surface of the nHA/Ag coating was approximately equal to that of the TC4 group, showing an accelerated proliferation pattern. Similarly, the cytoskeleton after 5 days of culture also presented the same result (Figure 9b).

Due to the higher requirements for antibacterial biomaterials and the need to meet biosafety requirements while meeting antibacterial properties, this study used an osteoblast-like cell line (MC3T3-E1) for the cytotoxicity test. The nHA/Ag-loaded coating was conducive to the adhesion of osteoblasts, and its morphology was normal, showing a spindle-shaped morphology, abundant pseudopods, and simulative cell proliferation (Figure 9). As verified, the cytotoxicity of AgNPs is concentration-dependent.[42] When the current

https://doi.org/10.1021/acsomega.1c04734
ACS Omega 2021, 6, 30027−30039

concentration is within a safe range, it not only shows no cytotoxicity but also promotes cell differentiation.[43] In summary, the Ag^+ concentration released by the nHA/Ag coating was within the range of biosafety, would not lead to the death of osteoblasts, and promoted cell proliferation and spreading on the surface over time.

Lactate dehydrogenase could be used to reflect the integrity of cell membranes, so the LDH enzyme release test was performed to further evaluate the state of osteoblasts on the coating surface (10a). In contrast, the MC3T3-E1 cells on the Ag coating expressed the highest LDH value, which meant that AgNPs could cause the stress response of osteoblasts and irreversibly cause cell membrane damage, while nHA could effectively reduce the toxicity of AgNPs and promote osteogenesis cell adhesion and spreading. Compared with polished TC4, nHA/Ag did not increase the LDH activity, indicating that there was no cytotoxicity. In general, the production of ROS in osteoblasts was quantitatively detected (Figure 10b). Consistent with the LDH results, the Ag coating presented the highest amount of ROS, which meant that AgNPs could induce the generation of reactive oxygen radicals in osteoblasts, and there was a hidden risk of cytotoxicity. In contrast, the nHA/Ag group displayed a relatively low amount of the ROS value, which was beneficial to the biocompatibility of the nHA/Ag coating. The results of LDH and ROS (Figure 10) presented that the surface cell structure of the cells on the SF-based coating was normal, and the active oxygen free radicals and lactate dehydrogenase were not stimulated by stress, indicating that the coating owned satisfactory biological activity and was beneficial to the adhesion, proliferation, and further osteogenic differentiation of osteoblasts on the surface. Then, the capability of MC3T3 cells developing a cytoskeleton was inspected, as displayed in Figure 10c. After incubating for 1 day, the cells on the nHA/Ag coating were strongly adhered and well spread with pore-associated filopodia, while those on the Ag coating showed sparse adhesion and relatively weak filopodia. Other than that, cells on TC4 and nHA were well extended and homogeneously distributed. Compared with other groups, the osteoblasts on the surface of the nHA/Ag coating developed relatively strong stress fibers, and the stress fibers continued to assemble and mature in the next few days, and finally covered the entire coating surface after 3 days, which meant that the nHA/Ag coating did not affect the development of cell stress fibers and the maturation of the cytoskeleton. It should be pointed out that the cell morphology of the Ag^+ coating surface of 1 day was significantly different from that of other groups. The analysis might be caused by the following two reasons: On the one hand, due to the stimulating effect of Ag^+ on osteoblasts, related research pointed out[44] that Ag^+ could cause abnormal cell proliferation, enlarged nucleus, obvious changes in the cell morphology, and scattered situations. On the other hand, the possible cause was the different cell types selected. MC3T3-E1 belongs to bone tumor cells. There was a tendency of abnormal proliferation and abnormal changes in the morphology, and it was more sensitive to different growth environments.

In summary, HA exists in natural bone in the form of nanoscale plates or rods, and the nanoscale thickness and length endow it with many important biological properties.[45] Therefore, the combination of nHA and SF could highly mimic the microstructure of natural bone, and nHA gave the functional coating better bone regeneration ability and rapid formation of mineralized deposits on the surface.[46] Compared with HA, nHA has a higher specific surface area and nanometer properties, which can improve the density, mechanical strength, and toughness of functional coatings.[47] In addition, nHA has been proven to have appropriate biocompatibility, osteogenesis, and angiogenesis activity, and it is conducive to the adhesion, proliferation, and differentiation of osteoblasts, serving as a promising orthopedic biomedical material.[48,49] However, the easy agglomeration, the poor flexibility, and the difficulty of desired shape formation greatly limit its application, especially for the treatment of bone defects in load-bearing parts. To overcome the abovementioned shortcomings, nHA is mixed with other polymers (such as SF) for surface modification of hard tissue implants to improve bone-promoting activity..[50,51] It is well known that nHA and collagen are widely used materials in bone repair. The combination of the two can highly mimic the microstructure of natural bone. For instance, an nHA/collagen composite scaffold is a good candidate for bone repair and regeneration and significantly improves the bone healing process.[52,53] Compared with collagen, SF has a wide range of sources, and its structure is easier to control and has a wide range of application prospects for forming composite biomaterials with nHA.[54] As verified, the obtained SF/ nHA composite material presented appropriate biocompatible ability to osteoblast[55] and tissue, acting as a good candidate for supporting bone regeneration.[56−58] The results of *in vitro* osteogenic experiments displayed that compared with SF, SF/nHA shows significantly increased ALP expression, collagen secretion and mineralization deposition, and increased expression of genes related to osteogenesis (Runx2 and osteocalcin).[59] The cDNA test showed that nHA affected the gene expression of bone mesenchymal stem cells (BMSCs) through the interleukin 1α autocrine/paracrine signal circuit and promoted differentiation.[60] It should be pointed out that many trace elements play an important role in bone formation. The nHA/SF composite coating can efficiently adsorb trace elements in the solution to form a highly bioactive surface enriched with trace elements.[61]

Many studies have shown that compared with bare-metal implants, coatings made of SF have been shown to significantly improve cell compatibility and induce differentiation.[62] In previous studies, we introduced the SF coating with antibiotics and nanosilver on Ti substrates and proved that it improves cell compatibility and the ability to induce osteogenic differentiation.[31] Here, we focus on in vitro evaluation, including cell spreading, toxicity, and stress response. It is reported that a coating containing nHA can quickly induce the formation of bony apatite in SBF and improve cell compatibility.[10] The surface is densely covered by a new apatite layer, indicating that nHA has good bone activity. MC3T3-E1 cells are commonly used to evaluate cell response to coating, including cell attachment, proliferation, and differentiation. The adhesion and spreading of cells on the surface of the bone bionic coating were significantly better than that of the control group. After culturing for 3 days, the cytoskeleton staining displayed that the osteoblasts spread normally. Meantime, ROS and LDH evaluated the stress response of the cells to the SF-based coating. The results showed that the addition of nHA can significantly improve the biological safety and biological activity of the composite coating. It is worth mentioning that when the release rate of Ag^+ was controlled to form a local low-concentration environment, not only would it not cause damage and toxicity to osteoblasts but it would promote cell proliferation and

https://doi.org/10.1021/acsomega.1c04734
ACS Omega 2021, 6, 30027−30039

differentiation, showing positive biological characteristics. Our study also confirmed that the formation of an nHA/AgNP complex showed a great impact on the biosafety and bioactivity of the coating. In future research, animal experiments are needed to study the interaction between the bone biomimetic SF-based coating and bone tissue, which is essential for preclinical evaluation.

One of our main goals is to develop a cost-effective, affordable, and easy-to-obtain bioactive coating that is specifically used for osteogenesis and can be used for implant infection prevention and bone tissue regeneration. Because nHA and SF are similar to the inorganic components and collagen fibers of bone tissue, they can significantly promote the osteogenic differentiation of cells. Therefore, the bone tissue bionic coating can be considered as a safe and promising coating for hard tissue implantation. As the most widely used hard-tissue implant in clinical practice, the infection caused by bacteria after the titanium-based implant is implanted in the body has always been the most difficult problem. The infection would not only lead to implantation failure but also revision and even concurrent infections in other parts. Therefore, imparting antibacterial ability and bone-forming activity to the titanium-based implant surface has important clinical significance. In this study, the HA/AgNP-loaded SF-based coating not only confirmed its superior antibacterial ability in *in vitro* experiments but also guaranteed that the biological safety and biological activity of the coating could promote the adhesion, spreading, and osteogenic differentiation of cells on the surface, and it has broad clinical application prospects.

3. CONCLUSIONS

A biomimetic method was used to synthesize nHA and silver nanoparticles with SF as a template, and the TC4 substrate was covered by dip coating. It was found that the obtained coating was dense and uniform, the hydrophilicity was significantly improved, and it had a good ability to inhibit the adhesion of bacteria and kill the floating bacteria. *In vitro* cell tests showed that the nHA/AgNP-loaded SF-based coating displayed good cytocompatibility, which was conducive to the adhesion and spreading of osteoblast MC3T3-E1 on the surface. LDH and ROS tests presented that the functional coating did not cause a severe cellular stress response. Therefore, the nHA/Ag-loaded SF-based coating owned both antibacterial and biological safety. It is a potentially effective solution to the postoperative infection and poor osseointegration of bare titanium implants and has a good clinical application prospect.

4. EXPERIMENTAL DETAILS

4.1. Materials. Silkworm cocoons (Bombyx mori) were purchased from Kyebong Farm (Cheongyang, Korea). Hydroxyapatite (HAp) and silver nitrate were purchased from CGBio and Sigma-Aldrich (St Louise, MO), respectively. All reagents used in the experiment were of high-performance liquid chromatography (HPLC) grade.

4.2. Preparation of a Silk Fibroin (SF) Solution. Natural silkworm cocoons were cut with scissors, 5 g of the cocoons was collected, and cooked for 30 min with a 0.02 M Na_2CO_3 solution to achieve the purpose of removing the sericin from the silkworm cocoons. The silk fibroin obtained after degumming was washed with deionized water to remove impurities and adsorbed ions, dried overnight, and then, dissolved in a 9.3 M LiBr solution for 1.5 h (60 °C). The yellow viscous liquid obtained after the dissolution was dialyzed with a dialysis membrane (3500 W) for 3 days, during which the deionized water was replaced every 8 h. After the dialysis, the solution was collected in a centrifuge tube and centrifuged at 4000 rpm for 20 min. The collected supernatant was the silk fibroin solution. The mass volume fraction was tested to be 10 w/v %, and it was diluted to 5% with deionized water. It was next stored in a refrigerator at 4 °C for later use.

4.3. Preparation of an SF/nHA/Ag Composite Solution. The transparent SF/nHA/Ag mixture solution was cultivated by adding nHA powder (2 mg) and $AgNO_3$ (2 mM) to 2 mL of a 5 wt % SF solution, and the final concentrations of nHA and Ag^+ in the solution, respectively, were 1 mg/L and 1 mM/L. Subsequently, the obtained SF/nHA/Ag solution was placed under an ultraviolet lamp (40W, Philips) and incubated at room temperature for 1 h to obtain the SF/nHA/Ag composite solution. Finally, the SF/nHA/Ag composite solution was stocked at 4 °C for further use.

4.4. Building of SF-Based Coatings on TC4. TC4 square slices (10 mm × 10 mm × 0.5 mm) were mechanically polished to a 2000 grain size and washed sequentially in acetone, ethanol, and deionized water (DI) for 15 min. Then, the squares were dried by a hairdryer. The functional coatings of nHA, Ag, and nHA/Ag were obtained by dropping SF, SF/AgNPs, and SF/AgNPs/gen solutions on the surface of the square piece by means of a simple spin-coating process.

4.5. Surface Characterization. The microstructure of the composite coating solution was characterized using a Hitachi1-9000 NAR transmission electron microscope (Hitachi, Japan). The physical morphology of the surface after coating was observed using a scanning electron microscope (SEM). An atomic force microscope (AFM, Dimension Icon, Bruker, America) was used to measure the average roughness (Ra) and root-mean-square roughness (Rq) of the polished and coated samples. X-ray photoelectron spectroscopy (XPS, ESCALAB 250Xi, Thermo Scientific, America) was used to analyze the elemental composition and the chemical state of the coating. The surface wettability after coating was measured using a contact angle goniometer (DO4222Mk1, Kruss, Germany) at room temperature. An amount of 5.0 μL of deionized water was dropped onto the surfaces of polished and dealloyed samples in five different places; then, the image was captured and the contact angle was measured. The chemical composition of the coating surface was characterized by a Fourier transform infrared spectrometer (FTIR, Nicolet, Madison, WI) in the range of 700−4000 cm^{-1}.

4.6. Cell Culture. Mouse osteoblasts (MC3T3-E1, Shanghai Institute of Biochemistry and Cell Biology, Chinese Academy of Sciences) were used to evaluate the biocompatibility of the coating. MC3T3-E1 was cultured in a humidified atmosphere of 37 °C and 5% CO_2 in an α-minimum essential medium (α-MEM, Hyclone) supplemented with a medium that contained 10% FBS and 1% penicillin/streptomycin (PS, Solarbio) and needed to be changed every 3 days. Before cell seeding, both sides of the sample were irradiated with ultraviolet light (UV) for 30 min. Then, the sample was placed in a 24-well TCPS; at the same time, MC3TC-E1 cells were seeded on TC4 with different coatings at a density of about 4×10^4 cells per well.

4.6.1. Cell Adhesion Assay. SEM and fluorescence microscopy were used to observe the adhesion and proliferation of MC3T3-E1 cells on the coating surface. First, the MC3TC-E1 cells were cultured on the surface of the

https://doi.org/10.1021/acsomega.1c04734
ACS Omega 2021, 6, 30027−30039

sample for 1, 3, and 5 days, and then, the medium was removed. After fixing and dehydrating, SEM was used to observe the shape of cells adhered to different coatings by sputter-coating gold. After 6 h of cocultivation, the cytoskeletal actin fibers were stained by FITC (5 μg/mL, Solarbio), and DAPI (10 μg/mL, Solarbio) was used to stain the nuclei. Finally, samples were examined under a fluorescence microscope.

4.6.2. Cell Cytotoxicity Assay. A lactate dehydrogenase kit (LDH, Solarbio) was used to evaluate the cytotoxicity of coatings. After 1, 3, and 5 days of cocultivation, the OD value of the cell lysate was measured at 450 nm using a microplate reader.

4.6.3. Cell Proliferation Assay. A CCK-8 kit (Tojin Institute of Chemical Technology, Japan, Dojindo) was used to measure the activity of cell mitochondria. After cocultivation for 1, 3, and 5 days, the new medium containing 10% CCK-8 was added and placed in an incubator for 1 h. The OD value of the medium was measured at 450 nm using a microplate reader.

4.7. Antimicrobial Activity Assays. *4.7.1. Bacteria Culture and Inoculation.* Under sterile conditions, *S. aureus* was cultured in Luria Bertani (LB) broth at 37 °C for 12 h, and then, the activated bacteria (106−107 CFU/mL) were cocultured with the samples (sterilized by UV) according to the predesigned time period.

4.7.2. Microbial Viability Assay. To study the ability of coatings to inhibit bacterial invasion, a WST Microbial Viability Assay Kit (WST, Dojindo, Japan) was used to measure bacterial mitochondrial metabolic activity. The new LB medium with 20% WST working solution was added to the sample and incubated in the dark for a specified time. The absorbance was measured at 450 nm using a microplate reader.

4.7.3. Characterization of Adherent Bacteria. After being fixed with 2.5% glutaraldehyde (GA), dehydrated in continuous ethanol (50−100%), and sprayed with gold, the morphology of the anchored bacteria was observed by SEM. *Staphylococcus aureus* on the coating was stained with a Live/Dead BacLight Bacterial Viability Kit (Invitrogen) to visualize the survival status of bacteria. After rinsing coatings, 1 mL of staining mix (6 μM SYTO 9; 30 μM propidium iodide (PI)) was added and kept in the dark for 15 min. CLSM was used to observe the final fluorescence image.

4.8. Statistical Analysis. All data in this study were analyzed using SPSS 19.0 software. Statistical significance was determined using one-way analysis of variance (ANOVA) or Student's *t* test. A *p* value of less than 0.05 was determined to be statistically significant. Data values are expressed as mean ± standard deviation.

AUTHOR INFORMATION

Corresponding Authors

Yunpeng Zhang − *Heping Hospital Affiliated to Changzhi Medical College, Changzhi 046000 Shanxi, China*; Email: yunpengz0625@163.com

Wenhao Zhou − *Shaanxi Key Laboratory of Biomedical Metal Materials, Northwest Institute for Non-ferrous Metal Research, Xi'an 710016, China*; Email: zwhpeking@gmail.com

Authors

Xiaorong Chen − *Changzhi Medical College, Changzhi 046000 Shanxi, China*

Yuan Li − *Heping Hospital Affiliated to Changzhi Medical College, Changzhi 046000 Shanxi, China*

Tian Bai − *Shaanxi Key Laboratory of Biomedical Metal Materials, Northwest Institute for Non-ferrous Metal Research, Xi'an 710016, China*

Chen Li − *Changzhi Medical College, Changzhi 046000 Shanxi, China*

Lingyan Jiang − *Heping Hospital Affiliated to Changzhi Medical College, Changzhi 046000 Shanxi, China*

Yu Liu − *Heping Hospital Affiliated to Changzhi Medical College, Changzhi 046000 Shanxi, China*

Changying Sun − *Heping Hospital Affiliated to Changzhi Medical College, Changzhi 046000 Shanxi, China*

Complete contact information is available at: https://pubs.acs.org/10.1021/acsomega.1c04734

Author Contributions

‖Y.Z. and X.C. contributed equally to this work.

Notes

The authors declare no competing financial interest.

ACKNOWLEDGMENTS

The authors acknowledge the financial support of the Project of Shanxi Province Health Commission Scientific Research (2019146) and the Foundation of Heping Hospital Affiliated to Changzhi Medical College Scientific Research (HPYJ201948)

REFERENCES

(1) Peitgen, D. S.; Innmann, M. M.; Merle, C.; Gotterbarm, T.; Moradi, B.; Streit, M. R. Cumulative long-term incidence of postoperative periprosthetic femoral fractures using an uncemented tapered titanium hip stem: 26-to 32-year results. *J. Arthroplasty* **2019**, *34*, 77−81.

(2) Mounir, M.; Atef, M.; Abou-Elfetouh, A.; Hakam, M. Titanium and polyether ether ketone (PEEK) patient-specific sub-periosteal implants: Two novel approaches for rehabilitation of the severely atrophic anterior maxillary ridge. *Int. J. Oral Maxillofac. Surg.* **2018**, *47*, 658−664.

(3) Yamako, G.; Janssen, D.; Hanada, S.; Anijs, T.; Ochiai, K.; Totoribe, K.; Chosa, E.; Verdonschot, N. Improving stress shielding following total hip arthroplasty by using a femoral stem made of β type Ti-33.6 Nb-4Sn with a young's modulus gradation. *J. Biomech.* **2017**, *63*, 135−143.

(4) Li, C.-Y.; Fan, X.-L.; Zeng, R.-C.; Cui, L.-Y.; Li, S.-Q.; Zhang, F.; He, Q.-K.; Kannan, M. B.; Jiang, H.-W. G.; Chen, D.-C.; et al. Corrosion resistance of in-situ growth of nano-sized $Mg(OH)_2$ on micro-arc oxidized magnesium alloy AZ31—Influence of EDTA. *J. Mater. Sci. Technol.* **2019**, *35*, 1088−1098.

(5) Stein, S.; Kruck, L.; Warnecke, D.; Seitz, A. M.; Dürselen, L.; Ignatius, A. Osseointegration of titanium with a novel silver coating under dynamic loading. *Eur. Cells Mater.* **2020**, *39*, 249−259.

(6) López-Valverde, N.; Sousa, B. M.-d.; López-Valverde, A.; Ramírez, J. M. Effectiveness of antibacterial surfaces in osseointegration of titanium dental implants: a systematic review. *Antibiotics* **2021**, *10*, 360.

(7) Han, D.-L.; Yu, P.-L.; Liu, X.-M.; Xu, Y.-D.; Wu, S.-L. Polydopamine modified CuS@ HKUST for rapid sterilization through enhanced photothermal property and photocatalytic ability. *Rare Met.* **2021**, DOI: 10.1007/s12598-021-01786-1.

(8) Li, Y.; Yang, Y.; Li, R.; Tang, X.; Guo, D.; Qing, Ya.; Qin, Y. Enhanced antibacterial properties of orthopedic implants by titanium nanotube surface modification: a review of current techniques. *Int. J. Nanomedicine* **2019**, *14*, 7217−7236.

(9) de Oliveira, P. G. F. P.; de Melo Soares, M. S.; Silveira e Souza, A. M. M.; Taba, M., Jr.; Palioto, D. B.; Messora, M. R.; Ghiraldini, B.; Nunes, F. A. dS.; de Souza, S. L. S. Influence of nano-hydroxyapatite coating implants on gene expression of osteogenic markers and micro-CT parameters. An in vivo study in diabetic rats. *J. Biomed. Mater. Res. A* **2021**, *109*, 682−694.
(10) Ke, D.; Vu, A. A.; Bandyopadhyay, A.; Bose, S. Compositionally graded doped hydroxyapatite coating on titanium using laser and plasma spray deposition for bone implants. *Acta Biomater.* **2019**, *84*, 414−423.
(11) Pang, H.; Tian, H.; Qiu, S.; Wang, N.; Wang, Y.-Q. Progress of titanium strut for cervical reconstruction with nano-graphene oxide loaded hydroxyapatite/polyamide composite and interbody fusion after corpectomy with anterior plate fixation. *Artif. Cells, Nanomed., Biotechnol.* **2019**, *47*, 3094−3100.
(12) Ye, P.; Yu, B.; Deng, J.; She, R. F.; Huang, W. L. Application of silk fibroin/chitosan/nano-hydroxyapatite composite scaffold in the repair of rabbit radial bone defect. *Exp. Ther. Med.* **2017**, *14*, 5547−5553.
(13) Pillai, M. M.; Sathishkumar, G.; Houshyar, S.; Senthilkumar, R.; Quigley, A.; Shanthakumari, S.; Padhye, R.; Bhattacharyya, A. Nanocomposite-coated silk-based artificial conduits: The influence of structures on regeneration of the peripheral nerve. *ACS Appl. Bio Mater.* **2020**, *3*, 4454−4464.
(14) Lovati, A. B.; Lopa, S.; Bottagisio, M.; Talò, G.; Canciani, E.; Dellavia, C.; Alessandrino, A.; Biagiotti, M.; Freddi, G.; Segatti, F.; et al. Peptide-enriched silk fibroin sponge and trabecular titanium composites to enhance bone ingrowth of prosthetic implants in an ovine model of bone gaps. *Front Bioeng. Biotechnol.* **2020**, *8*, No. 563203.
(15) Yin, X.; Yan, L.; Hao, D. J.; Liu, S.; Yang, M.; He, B.; Liu, Z. Calcium alginate template-mineral substituted hydroxyapatite hydrogel coated titanium implant for tibia bone regeneration. *Int. J. Pharm.* **2020**, *582*, No. 119303.
(16) Midha, S.; Murab, S.; Ghosh, S. Osteogenic signaling on silk-based matrices. *Biomaterials* **2016**, *97*, 133−153.
(17) Wu, Z.; Meng, Z.; Wu, Q.; Zeng, D.; Guo, Z.; Yao, J.; Bian, Y.; Gu, Y.; Cheng, S.; Peng, L. Biomimetic and osteogenic 3D silk fibroin composite scaffolds with nano MgO and mineralized hydroxyapatite for bone regeneration. *J. Tissue Eng.* **2020**, *11*, 2041731420967791.
(18) Vetsch, J. R.; Paulsen, S. J.; Müller, R.; Hofmann, S. Effect of fetal bovine serum on mineralization in silk fibroin scaffolds. *Acta Biomater.* **2015**, *13*, 277−285.
(19) Wang, J.; Yu, F.; Qu, L.; Meng, X.; Wen, G. Study of synthesis of nano-hydroxyapatite using a silk fibroin template. *Biomed. Mater.* **2010**, *5*, No. 041002.
(20) Dong, Y.; Ye, H.; Liu, Y.; Xu, L.; Wu, Z.; Hu, X.; Ma, J.; Pathak, J. L.; Liu, J.; Wu, G. pH dependent silver nanoparticles releasing titanium implant: A novel therapeutic approach to control peri-implant infection. *Colloids Surf., B* **2017**, *158*, 127−136.
(21) Deng, L.; Deng, Y.; Xie, K. AgNPs-decorated 3D printed PEEK implant for infection control and bone repair. *Colloids Surf., B* **2017**, *160*, 483−492.
(22) Jia, Z.; Shi, Y.; Xiong, P.; Zhou, W.; Cheng, Y.; Zheng, Y.; Xi, T.; Wei, S. From solution to biointerface: graphene self-assemblies of varying lateral sizes and surface properties for biofilm control and osteodifferentiation. *ACS Appl. Mater. Interfaces* **2016**, *8*, 17151−17165.
(23) Wang, B.; Wu, Z.; Lan, J.; Li, Y.; Xie, L.; Huang, X.; Zhang, A.; Qiao, H.; Chang, X.; Lin, H.; et al. Surface modification of titanium implants by silk fibroin/Ag co-functionalized strontium titanate nanotubes for inhibition of bacterial-associated infection and enhancement of in vivo osseointegration. *Surf. Coat. Technol.* **2021**, *405*, No. 126700.
(24) Zhou, W.; Li, Y.; Yan, J.; Xiong, P.; Li, Q.; Cheng, Y.; Zheng, Y. Construction of self-defensive antibacterial and osteogenic AgNPs/gentamicin coatings with chitosan as nanovalves for controlled release. *Sci. Rep.* **2018**, *8*, No. 13432.
(25) Zhou, W.; Jia, Z.; Xiong, P.; Yan, J.; Li, M.; Cheng, Y.; Zheng, Y. Novel pH-responsive tobramycin-embedded micelles in nano-structured multilayer-coatings of chitosan/heparin with efficient and sustained antibacterial properties. *Mater. Sci. Eng., C* **2018**, *90*, 693−705.
(26) Lu, Q.; Zhu, H.; Zhang, C.; Zhang, F.; Zhang, B.; Kaplan, D. L. Silk self-assembly mechanisms and control from thermodynamics to kinetics. *Biomacromolecules* **2012**, *13*, 826−832.
(27) Ribeiro, M.; Ferraz, M. P.; Monteiro, F. J.; Fernandes, M. H.; Beppu, M. M.; Mantione, D.; Sardon, H. Antibacterial silk fibroin/nanohydroxyapatite hydrogels with silver and gold nanoparticles for bone regeneration. *Nanomedicine* **2017**, *13*, 231−239.
(28) Zhou, W.; Jia, Z.; Xiong, P.; Yan, J.; Li, Y.; Li, M.; Cheng, Y.; Zheng, Y. Bioinspired and biomimetic AgNPs/gentamicin-embedded silk fibroin coatings for robust antibacterial and osteogenetic applications. *ACS Appl. Mater. Interfaces* **2017**, *9*, 25830−25846.
(29) Pritchard, E. M.; Kaplan, D. L. Silk fibroin biomaterials for controlled release drug delivery. *Expert Opin. Drug Deliv.* **2011**, *8*, 797−811.
(30) Deligianni, D. D.; Katsala, N. D.; Koutsoukos, P. G.; Missirlis, Y. F. Effect of surface roughness of hydroxyapatite on human bone marrow cell adhesion, proliferation, differentiation and detachment strength. *Biomaterials* **2000**, *22*, 87−96.
(31) Wenhao, Z.; Zhang, T.; Yan, J.; Li, Q.; Xiong, P.; Li, Y.; Cheng, Y.; Zheng, Y. In vitro and in vivo evaluation of structurally-controlled silk fibroin coatings for orthopedic infection and in-situ osteogenesis. *Acta Biomat.* **2020**, *116*, 223−245.
(32) Li, B.; Webster, T. J. Bacteria antibiotic resistance: New challenges and opportunities for implant-associated orthopedic infections. *J. Orthop. Res.* **2018**, *36*, 22−32.
(33) Fu, J.; Li, Y.; Zhang, Y.; Liang, Y.; Zheng, Y.; Li, Z.; Zhu, S.; Li, C.; Cui, Z.; Wu, S. An engineered pseudo-Macrophage for rapid treatment of bacteria-Infected osteomyelitis via microwave-Excited anti-infection and immunoregulation. *Adv. Mater.* **2021**, *33*, No. 2102926.
(34) Zheng, Q.; Liu, X.; Zheng, Y.; Yeung, K. W.; Cui, Z.; Liang, Y.; Li, Z.; Zhu, S.; Wang, X.; Wu, S. The recent progress on metal−Organic frameworks for phototherapy. *Chem. Soc. Rev.* **2021**, *50*, 5086−5125.
(35) Barros, J.; Melo, L. D.; Poeta, P.; Igrejas, G.; Ferraz, M. P.; Azeredo, J.; Monteiro, F. J. Lytic bacteriophages against multidrug-resistant staphylococcus aureus, enterococcus faecalis and escherichia coli isolates from orthopaedic implant-associated infections. *Int. J. Antimicrob. Agents* **2019**, *54*, 329−337.
(36) Bryaskova, R.; Pencheva, D.; Nikolov, S.; Kantardjiev, T. Synthesis and comparative study on the antimicrobial activity of hybrid materials based on silver nanoparticles (AgNps) stabilized by polyvinylpyrrolidone (PVP). *J. Chem. Biol.* **2011**, *4*, 185−191.
(37) Ojo, O. A.; Oyinloye, B. E.; Ojo, A. B.; Afolabi, O. B.; Peters, O. A.; Olaiya, O.; Fadaka, A.; Jonathan, J.; Osunlana, O. Green synthesis of silver nanoparticles (AgNPs) using *talinum triangulare* (Jacq.) Willd. leaf extract and monitoring their antimicrobial activity. *J. Bionanosci.* **2017**, *11*, 292−296.
(38) Xiu, Z.-m.; Zhang, Q.-b.; Puppala, H. L.; Colvin, V. L.; Alvarez, P. J. Negligible particle-specific antibacterial activity of silver nanoparticles. *Nano Lett.* **2012**, *12*, 4271−4275.
(39) Mao, C.; Xiang, Y.; Liu, X.; Cui, Z.; Yang, X.; Yeung, K. W. K.; Pan, H.; Wang, X.; Chu, P. K.; Wu, S. Photo-inspired antibacterial activity and wound healing acceleration by hydrogel embedded with Ag/Ag@ AgCl/ZnO nanostructures. *ACS Nano* **2017**, *11*, 9010−9021.
(40) Kong, X.; Liu, X.; Zheng, Y.; Chu, P. K.; Zhang, Y.; Wu, S. Graphitic carbon nitride-based materials for photocatalytic antibacterial application. *Mater. Sci. Eng., Rep.* **2021**, *145*, No. 100610.
(41) Li, W.; Yang, Y.; Zhang, H.; Xu, Z.; Zhao, L.; Wang, J.; Qiu, Y.; Liu, B. Improvements on biological and antimicrobial properties of titanium modified by AgNPs-loaded chitosan-heparin polyelectrolyte multilayers. *J. Mater. Sci: Mater. Med.* **2019**, *30*, No. 52.

https://doi.org/10.1021/acsomega.1c04734
ACS Omega 2021, 6, 30027−30039

(42) Guo, J.; Qin, S.; Wei, Y.; Liu, S.; Peng, H.; Li, Q.; Luo, L.; Lv, M. Silver nanoparticles exert concentration-dependent influences on biofilm development and architecture. *Cell Prolif* **2019**, *52*, No. e12616.
(43) Patil, S.; Singh, N. Antibacterial silk fibroin scaffolds with green synthesized silver nanoparticles for osteoblast proliferation and human mesenchymal stem cell differentiation. *Colloids Surf., B* **2019**, *176*, 150−155.
(44) Jia, Z.; Xiu, P.; Li, M.; Xu, X.; Shi, Y.; Cheng, Y.; Wei, S.; Zheng, Y.; Xi, T.; Cai, H.; et al. Bioinspired anchoring AgNPs onto micro-nanoporous TiO_2 orthopedic coatings: trap-killing of bacteria, surface-regulated osteoblast functions and host responses. *Biomaterials* **2016**, *75*, 203−222.
(45) Wang, F.; Zhang, Y. C.; Zhou, H.; Guo, Y. C.; Su, X. X. Evaluation of in vitro and in vivo osteogenic differentiation of nano-hydroxyapatite/chitosan/poly (lactide-co-glycolide) scaffolds with human umbilical cord mesenchymal stem cells. *J. Biomed. Mater. Res. A* **2014**, *102*, 760−768.
(46) Hu, Y.; Cao, S.; Chen, J.; Zhao, Y.; He, F.; Li, Q.; Zou, L.; Shi, C. Biomimetic fabrication of icariin loaded nano hydroxyapatite reinforced bioactive porous scaffolds for bone regeneration. *Chem. Eng. J.* **2020**, *394*, No. 124895.
(47) Ma, J.; Li, Z.; Xue, Y.; Liang, X.; Tan, Z.; Tang, B. Novel PEEK/nHA composites fabricated by hot-pressing of 3D braided PEEK matrix. *Adv. Compos. Hybrid Mater.* **2020**, *3*, 156−166.
(48) Kim, M. H.; Yun, C.; Chalisserry, E. P.; Lee, Y. W.; Kang, H. W.; Park, S.-H.; Jung, W.-K.; Oh, J.; Nam, S. Y. Quantitative analysis of the role of nanohydroxyapatite (nHA) on 3D-printed PCL/nHA composite scaffolds. *Mater. Lett.* **2018**, *220*, 112−115.
(49) Chen, X.; Gao, C.; Jiang, J.; Wu, Y.; Zhu, P.; Chen, G. 3D printed porous PLA/nHA composite scaffolds with enhanced osteogenesis and osteoconductivity in vivo for bone regeneration. *Biomed. Mater.* **2019**, *14*, No. 065003.
(50) Abbasizadeh, N.; Rezayan, A. H.; Nourmohammadi, J.; Kazemzadeh-Narbat, M. HHC-36 antimicrobial peptide loading on silk fibroin (SF)/hydroxyapatite (HA) nanofibrous-coated titanium for the enhancement of osteoblast and bactericidal functions. *Int. J. Polym. Mater. Polym. Biomater.* **2020**, *69*, 629−639.
(51) Farokhi, M.; Mottaghitalab, F.; Samani, S.; Shokrgozar, M. A.; Kundu, S. C.; Reis, R. L.; Fatahi, Y.; Kaplan, D. L. Silk fibroin/hydroxyapatite composites for bone tissue engineering. *Biotechnol. Adv.* **2018**, *36*, 68−91.
(52) Li, M.; Li, L.; Su, K.; Liu, X.; Zhang, T.; Liang, Y.; Jing, D.; Yang, X.; Zheng, D.; Cui, Z.; et al. Highly effective and noninvasive near-infrared eradication of a *staphylococcus aureus* biofilm on implants by a photoresponsive coating within 20 min. *Adv. Sci.* **2019**, *6*, No. 1900599.
(53) Xie, X.; Mao, C.; Liu, X.; Tan, L.; Cui, Z.; Yang, X.; Zhu, S.; Li, Z.; Yuan, X.; Zheng, Y.; et al. Tuning the bandgap of photo-sensitive polydopamine/Ag_3PO_4/graphene oxide coating for rapid, noninvasive disinfection of implants. *ACS Cent. Sci.* **2018**, *4*, 724−738.
(54) Marelli, B.; Ghezzi, C. E.; Alessandrino, A.; Barralet, J. E.; Freddi, G.; Nazhat, S. N. Silk fibroin derived polypeptide-induced biomineralization of collagen. *Biomaterials* **2012**, *33*, 102−108.
(55) Wang, J.; Yang, Q.; Mao, C.; Zhang, S. Osteogenic differentiation of bone marrow mesenchymal stem cells on the collagen/silk fibroin bi-template-induced biomimetic bone substitutes. *J. Bio. Mater. Res. A* **2012**, *100A*, 2929−2938.
(56) Jin, Y.; Kundu, B.; Cai, Y.; Kundu, S. C.; Yao, J. Bio-inspired mineralization of hydroxyapatite in 3D silk fibroin hydrogel for bone tissue engineering. *Colloids Surf., B* **2015**, *134*, 339−345.
(57) Shen, X.; Zhang, Y.; Gu, Y.; Xu, Y.; Liu, Y.; Li, B.; Chen, L. Sequential and sustained release of SDF-1 and BMP-2 from silk fibroin-nanohydroxyapatite scaffold for the enhancement of bone regeneration. *Biomaterials* **2016**, *106*, 205−216.
(58) Liu, H.; Xu, G. W.; Wang, Y. F.; Zhao, H. S.; Xiong, S.; Wu, Y.; Heng, B. C.; An, C. R.; Zhu, G. H.; Xie, D. H. Composite scaffolds of nano-hydroxyapatite and silk fibroin enhance mesenchymal stem cell-based bone regeneration via the interleukin 1 alpha autocrine/paracrine signaling loop. *Biomaterials* **2015**, *49*, 103−112.
(59) Huang, X.; Bai, S.; Lu, Q.; Liu, X.; Liu, S.; Zhu, H. Osteoinductive-nanoscaled silk/HA composite scaffolds for bone tissue engineering application. *J. Biomed. Mater. Res., Part B* **2015**, *103*, 1402−1414.
(60) Alipour, M.; Firouzi, N.; Aghazadeh, Z.; Samiei, M.; Montazersaheb, S.; Khoshfetrat, A. B.; Aghazadeh, M. The osteogenic differentiation of human dental pulp stem cells in alginate-gelatin/nano-hydroxyapatite microcapsules. *BMC Biotechnol.* **2021**, *21*, No. 6.
(61) Ding, Z.; Fan, Z.; Huang, X.; Lu, Q.; Xu, W.; Kaplan, D. L. Silk−hydroxyapatite nanoscale scaffolds with programmable growth factor delivery for bone repair. *ACS Appl. Mater. Interfaces* **2016**, *8*, 24463−24470.
(62) Xiao, L.; Wu, M.; Yan, F.; Xie, Y.; Liu, Z.; Huang, H.; Yang, Z.; Yao, S.; Cai, L. A radial 3D polycaprolactone nanofiber scaffold modified by biomineralization and silk fibroin coating promote bone regeneration in vivo. *Int. J. Biol. Macromol.* **2021**, *172*, 19−29.

https://doi.org/10.1021/acsomega.1c04734
ACS Omega 2021, 6, 30027−30039